Electronic Supplementary Material (ESI) for Physical Chemistry Chemical Physics.

Supplementary Information

Different hydrogen bonding environments of the Retinal protonated Schiff base control the photoisomerization in Channelrhodopsin-2

Yanan Guo, [†a] Franziska E. Wolff, [a] Igor Schapiro, [b] Marcus Elstner [a,c] and Marco Marazzi *[a,d]

[a.] *Department of Theoretical Chemical Biology, Institute of Physical Chemistry, Karlsruhe Institute of Technology, Kaiserstrasse 12, 76131 Karlsruhe, Germany.*
[b.] *Fritz Haber Center for Molecular Dynamics Research, Institute of Chemistry, Hebrew University of Jerusalem, Aronberg, 128 Jerusalem, Israel.*
[c.] *Institute of Physical Chemistry & Institute of Biological Interfaces (IBG-2), Karlsruhe Institute of Technology, Kaiserstrasse 12, Karlsruhe 76131, Germany.*
[d.] *Departamento de Química, Centro de Investigación en Síntesis Química (CISQ), Universidad de La Rioja, Madre de Dios, 53, 26006 Logroño, Spain. E-mail: marco.marazzi@unirioja.es*
† Y. G. present address: State Key Laboratory of Material-Orientated Chemical Engineering, College of Chemistry and Chemical Engineering, Nanjing Tech University, Nanjing 210009, China.

Content

1. The QM/MM scheme and model setup

The Hamiltonian describing the QM/MM scheme, as implemented in the Molcas software and used in this study by the Molcas/Tinker interface, is as following:

$$H = H_{QM} + H_{MM} - \sum_{i=1}^{n}\sum_{j=1}^{m}\frac{q_j}{r_{ij}} + \sum_{i=1}^{n}\sum_{j=1}^{m}\frac{Z_i q_j}{R_{ij}} + E_{QM/MM}^{vdW} + E_{QM/MM}^{bonded}$$

where H_{QM} describes the QM segment and H_{MM} the MM segment. The remaining terms represent the interactions between the QM and MM segments: (1) the third term describes the electrostatic interactions between QM electrons and MM point charges (q_j); *i* is the index of the electron, *n* the total number of electrons, *j* the index of the MM point charge, *m* the total number of MM point charges, r_{ij} the electron–MM point charge distance. (2) The forth term describes the electrostatic interactions between QM nuclei and MM point charges (q_j); *N* is the total number of atoms, Z_i the nucleus charge, R_{ij} nucleus–MM point charge distance. (3) The fifth term describes the short-range van der Waals interactions. (4) The last term includes the additionally parametrized potentials required to correctly describe QM/MM frontier. The QM wavefunction is polarized by the MM point charges. In contrast, the MM point charges remain constant during the calculation. The frontier QM atom N is saturated with a hydrogen link atom (HLA). The link atom is fixed at 1 Å from N and kept along the N-Cε axis throughout all calculations. The QM/MM partition applied in this study is shown in Figure S1.

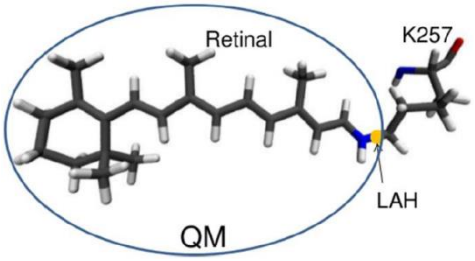

Figure S1. The QM/MM partition in the current calculations. The QM-MM frontier was placed at the N-Cε bond connecting the K257 side chain and the retinal. The frontier QM atom N is saturated with a hydrogen link atom (HLA).

In the Charmm22 force field, each amino acid residue has a net charge. For instance, the lysine (K) has a net charge of +1 representing a protonated residue. In the current QM/MM framework, the point charges of K257 (the lysine covalently linked to the retinal chromophore, *i.e.* to $RSBH^+$) are modified (see Table S1) to avoid the over polarization of the QM segment by the MM segment. More in detail, the point charges of Cε and two Hε atoms are set to zero, and these charges are redistributed equally on the remaining MM atoms of K257.

The $RSBH^+$ counterions E123 and D253 are deprotonated; the remaining titrable residues are assigned with the standard protonation states of the Charmm22 force field, except E90 and D156 which are set to be protonated. Three chloride ions were added to keep the system neutral.

Table S1. The values of the reparametrized QM/MM point charges for K257.

Atom	N	H_N	C_α	H_α	$C_{carbonyl}$	$O_{carbonyl}$	C_β
Charge	-0.33876	0.28384	-0.23086	0.15174	0.74324	-0.58026	-0.00026
Atom	H_β	C_γ	H_γ	C_δ	H_δ	C_ε	H_ε
Charge	0.04524	-0.10193	0.03699	0.02698	0.03472	0.0000	0.0000

2. Equilibration Steps Prior to the FTIR Spectrum Calculation

All steps were performed with the SCC-DFTB/Charm22 level of theory. Firstly, the geometry is optimized using the Conjugate Gradient (CONJ) minimizer until a gradient threshold of 1×10^{-3} a.u. is reached and, subsequently, using the Newton–Raphson (ABNR) minimizer with a gradient threshold of 1×10^{-5} a.u. Then the system is subjected to a heating (NVT) and pressure (NPT) MD equilibration. The resulting equilibrated structure is subject to an NPT production run of 2 ns. The time step is 0.5 fs. During the production run, the dipole moments needed to generate the FTIR spectrum are collected at each time step. Subsequently, the Fourier transform of the dipole moment autocorrelation function is computed to obtain the spectrum from each trajectory.

3. Ground State Optimized Geometries

In order to get optimal structures before starting the excited state calculations, the three models were optimized on the ground state at the B3LYP/MM and the CASSCF/MM levels of theory. The results are shown in Figure S2, where it can be seen how the initial $RSBH^+$-D253 $RSBH^+\cdots{}^-O$-(D253) model is converted in a $RSBH^+\cdots OH_2$ model after QM/MM optimization.

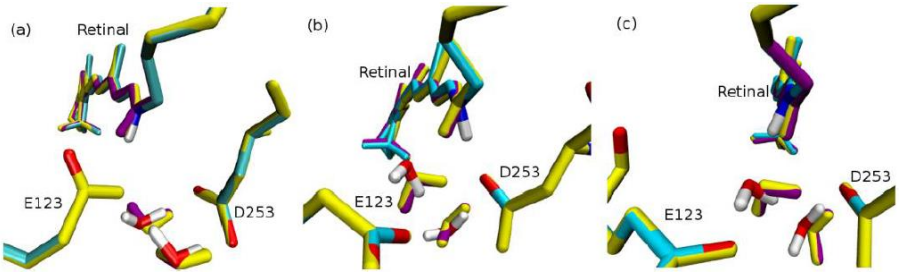

Figure S2. Superposition of the ground state CASSCF/MM geometry (yellow), B3LYP/MM geometry (purple) and the initial geometry from the previous MD simulation (cyan). (a) $RSBH^+\cdots{}^-$O-(E123) model, (b) $RSBH^+\cdots{}^-$O-(D253) model, (c) $RSBH^+\cdots OH_2$ model.

Hence, we further characterized the retinal conjugated polyene chain bond length (Figure S3), curvature (Figure S4) and helicity (Figure S5) of $RSBH^+\cdots{}^-$O-(E123) and $RSBH^+\cdots OH_2$ models. The $RSBH^+\cdots{}^-$O-(D253) model is not shown, since it resembles the $RSBH^+$-H_2O model, as explained above and in the main text.

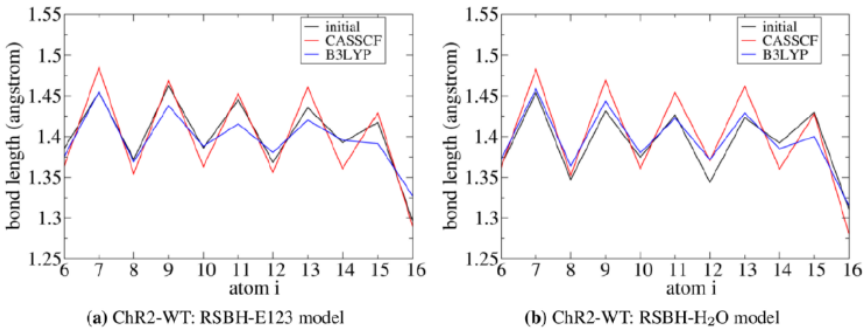

Figure S3. The retinal polyene chain bond length of the CASSCF/MM, B3LYP/MM and initial geometries.

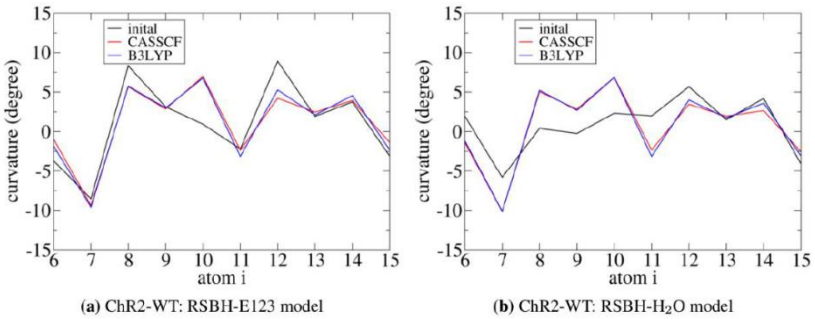

Figure S4. The retinal polyene chain curvature of the CASSCF/MM, B3LYP/MM and initial geometries.

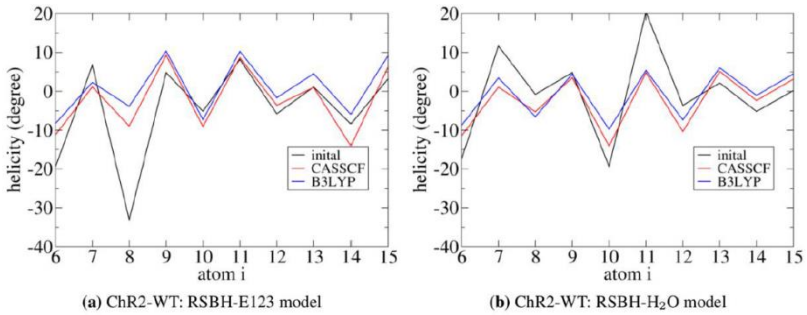

Figure S5. The retinal polyene chain helicity of the CASSCF/MM, B3LYP/MM and initial geometries.

As we can see, the bond length alternation of the B3LYP/MM optimized geometry is slightly smaller than that at CASSCF/MM level. This means that using the B3LYP functional results in stronger retinal polyene chain conjugation than using the CASSCF method, as expected. No significant changes in the backbone curvature and planarity are observed between B3LYP/MM and CASSCF/MM geometries. As a conclusion, the B3LYP and CASSCF approaches result in quite similar retinal backbone geometries for the current models.

4. Photoisomerization Pathway of the RSBH$^+$···$^-$O-(D253) Model

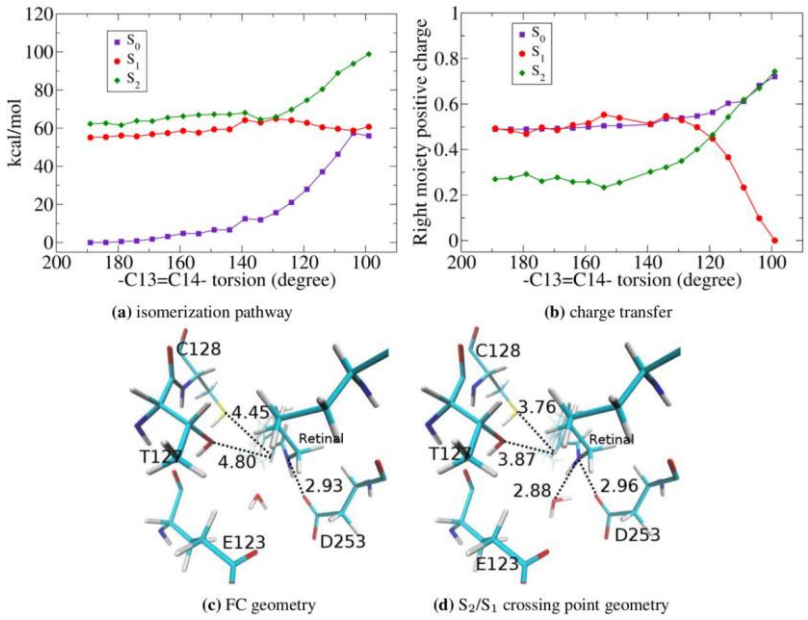

Figure S6. (a) The retinal isomerization pathway and (b) the Mulliken charge along the isomerization coordinate of the RSBH$^+$···$^-$O-(D253) model, considering the initial structure prior to ground state QM/MM optimization. (c) The FC and (d) the S_2/S_1 crossing geometries are shown. The dotted lines represent the hydrogen bonds. The distance are shown in Å.

5. Molecular Orbitals

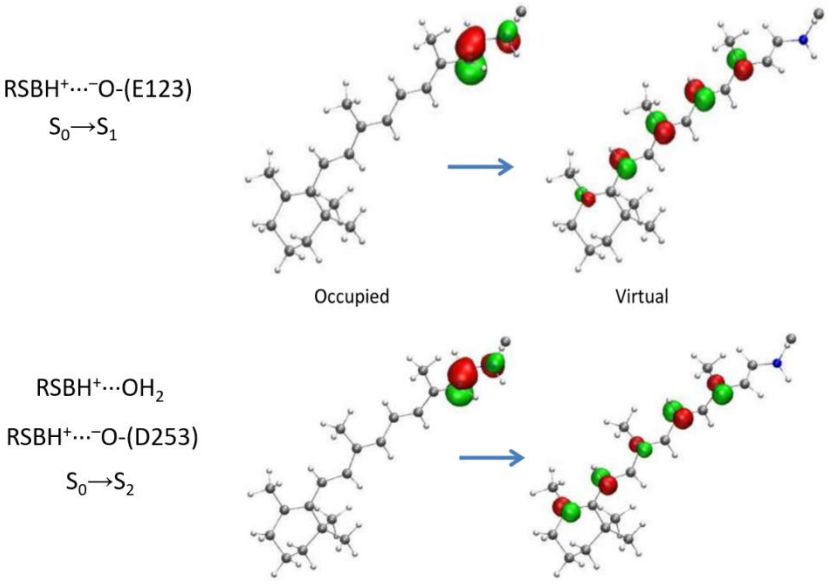

Figure S7. CASSCF molecular orbitals mainly involved in the $S_0 \rightarrow S_1$ vertical electronic transition of the RSBH$^+$···$^-$O-(E123) pattern, and in the $S_0 \rightarrow S_2$ vertical electronic transition of the RSBH$^+$···$^-$O-(D253) and RSBH$^+$···OH$_2$ patterns. Charge transfer occurs from the Schiff base toward the β-ionone ring, along the polyene chain.

6. CASPT2 Parameters and Franck-Condon Vertical Transition Energies

The vertical excitation energies of the CASSCF ground state optimized models were calculated by multi-state (MS) and state-specific (SS) CASPT2 levels of theory, keeping the IPEA parameter at 0.0. The results are shown in Table S2.

Table S2. CASSCF energies (E_{CASSCF}, in eV), SS-CASPT2 energies ($E_{SS\text{-}CASPT2}$, in eV), MS-CASPT2 energies ($E_{MS\text{-}CASPT2}$, in eV) and the CASPT2 oscillator strengths (f) for S_0 geometries optimized. S_0 is defined as the zero-energy state. The experimental absorption maximum is 2.62 eV (473 nm). IPEA shift = 0.0.

Pattern	*State*	E_{CASSCF}	$E_{SS\text{-}CASPT2}$	$E_{MS\text{-}CASPT2}$	$f_{SS\text{-}CASPT2}$	$f_{MS\text{-}CASPT2}$
RSBH$^+$···$^-$O-(E123)	S_0	0	0	0		
	S_1	3.91	3.05	2.93	0.68	1.65
	S_2	4.46	3.84	4.18	0.67	0.16
RSBH$^+$···OH$_2$	S_0	0	0	0		
	S_1	4.22	3.52	3.16	0.29	0.31
	S_2	4.74	3.70	4.35	1.02	1.52
RSBH$^+$···$^-$O-(D253)	S_0	0	0	0		
	S_1	3.62	3.02	2.91	0.14	0.44
	S_2	4.10	3.20	3.12	1.19	1.82

As it can be seen, both SS- and MS-CASPT2 levels of theory are in agreement, with the MS-CASPT2 energies more near to the experimental value. Hence, the MS-CASPT2 level was used to correct the CASSCF energies all along the photoisomerization pathways.

Moreover, in the Molcas code the zero-th order Hamiltonian can be modified with the so-called IPEA shift, an empirical correction introduced in 2004. Especially, in Table S3 the absorption values of the QM/MM optimized geometries are shown, when using the default IPEA shift of 0.25.

Table S3. SS-CASPT2 energies ($E_{SS\text{-}CASPT2}$, in eV), MS-CASPT2 energies ($E_{MS\text{-}CASPT2}$, in eV) and the CASPT2 oscillator strengths (f) for S_0 geometries optimized. S_0 is defined as the zero-energy state. IPEA shift = 0.25.

Pattern	*State*	$E_{SS\text{-}CASPT2}$	$E_{MS\text{-}CASPT2}$	$f_{SS\text{-}CASPT2}$	$f_{MS\text{-}CASPT2}$
RSBH$^+$···$^-$O-(E123)	S_0	0	0		
	S_1	3.10	2.98	0.71	1.68
	S_2	4.24	4.59	0.77	0.25
RSBH$^+$···OH$_2$	S_0	0	0		
	S_1	3.58	3.21	0.32	0.34
	S_2	4.11	4.77	1.11	1.62
RSBH$^+$···$^-$O-(D253)	S_0	0	0		
	S_1	3.09	2.97	0.17	0.47
	S_2	3.63	3.52	1.29	1.91

As it can be seen, when comparing Tables S2 and S3, the effect of the IPEA shift corresponds to a larger energy shift between ground and excited states (*ca.* 0.05 eV for S_0-S_1 and *ca.* 0.40 eV for S_0-S_2). Also, the oscillator strengths are higher when introducing the IPEA shift (*ca.* 0.03 for S_0-S_1 and *ca.* 0.10 for S_0-S_2).